



# Fabrication of Fe-doped WO<sub>3</sub> films for NO<sub>2</sub> sensing at lower operating temperature



T. Tesfamichael<sup>a,\*</sup>, C. Piloto<sup>a</sup>, M. Arita<sup>b</sup>, J. Bell<sup>a</sup>

<sup>a</sup> Science and Engineering Faculty, Queensland University of Technology, 2 George Street, Brisbane 4000, QLD Australia

<sup>b</sup> Laboratory of Nanoscience and Materials, Hokkaido University, Kita 14, Nishi 9, Kita-Ku, Sapporo 060-0814, Japan

## ARTICLE INFO

### Article history:

Received 5 January 2015

Received in revised form 20 April 2015

Accepted 23 June 2015

Available online 28 June 2015

### Keywords:

Nanostructure thin films  
Tungsten oxide  
Fe-doping  
Optical band gap  
NO<sub>2</sub> gas sensing  
Low operating temperature

## ABSTRACT

Fe-doped tungsten oxide thin films with different concentrations (0–2.6 at%) were synthesized on glass and alumina substrates at room temperature using DC reactive sputtering and subsequently annealed at 300 °C for 1 h in air. The alumina substrate has pre-printed interdigitated Pt-electrodes for gas sensing measurements. The effects of Fe-doping on the film structure and morphology, electronic and optical properties for gas sensing were investigated. The grain size of the different films on the alumina and Pt regions of the substrate vary only slightly between 43 and 57 nm with median size of about 50 nm. Raman spectra showed that the integrated intensity of W=O to O–W–O bands increases with increasing Fe concentrations and this indicated an increase in the number of defects. From XPS the different concentrations of the Fe-doped films were 0.03 at%, 1.33 at% and 2.6 at%. All the films deposited on glass substrate have shown similar visible transmittance (about 70%) but the optical band gap of the pure film decreased from 3.30 eV to 3.15 eV after doping with 2.6 at% Fe. The Fe-doped WO<sub>3</sub> film with the highest Fe concentration (2.6 at% Fe) has shown an enhanced gas sensing properties to NO<sub>2</sub> at relatively lower operating temperature (150 °C) and this can be attributed to the decrease in the optical band gap and an increase in the number of defects compared to the pure WO<sub>3</sub> film.

© 2015 Elsevier B.V. All rights reserved.

## 1. Introduction

Thin film deposition process is one of the most critical stages when manufacturing advanced devices such as microprocessors, solar cells, lasers, gas sensors, etc. Precise control of film processes with optimal film properties is of paramount importance for a specific application [1]. Various techniques have been used to deposit nanostructured metal oxide thin films including sol–gel, chemical vapour deposition, advanced gas deposition, and physical vapour deposition [2–7]. Each of the film deposition techniques has its own advantages and limitations but a better film quality and properties may be obtained using physical vapour deposition (PVD) techniques. Among the various PVD techniques, DC magnetron sputtering has the advantages of higher deposition rate and simplified fabrication steps to obtain nanostructured thin films of desired properties. Nanostructured materials have very large surface-to-volume ratio which are suitable for gas sensors as they offer more surface-to-gas interaction and thereby enhance sensing performance.

Thin films of tungsten oxide (WO<sub>3</sub>) has become a promising material for sensing various gases such as NO<sub>2</sub>, NH<sub>3</sub>, H<sub>2</sub>S, CO and ethanol due to the material's inherent electrical resistivity and excellent sensitivity and selectivity. The sensor response can be enhanced by modifying the film properties including grain size, film thickness, film porosity, surface morphology, impurities such as dopants or metal inclusions, crystallinity, defects and film stoichiometry [8,9]. From a theoretical study by Wang et al. [10], sensor response can be significantly enhanced if the grain size is smaller than 50 nm. A 2–3 order of magnitude increase in response was observed in the case of In<sub>2</sub>O<sub>3</sub> films when the grain size was decreased from 60–80 nm to less than 50 nm [11]. Sensors composed of WO<sub>3</sub> nanotubes have also shown enhanced response to NO<sub>2</sub> due to the large surface area presented by the interior of the nanotube assemblies [12].

Dopants are important for the formation of oxygen vacancies and modification of the electronic structure and band gap energy of metal oxides. It has been shown elsewhere [1,13–18] that metal inclusion in the oxide matrix increased the response to specific gases. Consumption of oxygen adsorbents on the metal, in addition to those on the metal oxide surface, by reaction with gas, causes enhanced sensor response. Tungsten oxide film doped with Pd has shown high response and selectivity towards hydrogen gas at a

\* Corresponding author.

E-mail address: [t.tesfamichael@qut.edu.au](mailto:t.tesfamichael@qut.edu.au) (T. Tesfamichael).

**Table 1**Input parameters (power, pressure (*P*), temperature (*T*) and time) used during deposition of pure and Fe-doped WO<sub>3</sub> films on glass and alumina substrates.

| Specimen                       | W-sputtering power (W) | Fe-sputtering power (W) | <i>T</i> (°C) | <i>P</i> (Pa) | Sputtering time (min) |
|--------------------------------|------------------------|-------------------------|---------------|---------------|-----------------------|
| Pure WO <sub>3</sub>           | 40                     | 0                       | 24            | 1.60          | 75                    |
| WO <sub>3</sub> :Fe (0.03 at%) | 40                     | 5                       | 24            | 1.60          | 75                    |
| WO <sub>3</sub> :Fe (1.33 at%) | 40                     | 20                      | 24            | 1.60          | 75                    |
| WO <sub>3</sub> :Fe (2.6 at%)  | 40                     | 40                      | 24            | 1.60          | 75                    |

working temperature of 200 °C [19]. The response of WO<sub>3</sub> films to H<sub>2</sub>S has been improved when doping with Au, while doping of the film with Ag and Pt showed higher responses to NO<sub>2</sub> and NH<sub>3</sub>, respectively [20]. Studies have shown addition of Cu to WO<sub>3</sub> thin film improved the sensor response when exposed to NO<sub>2</sub> whereas addition of Fe caused to increase the response towards ozone, CO and ethanol [21]. Defects such as oxygen vacancies are inherent in metal oxides and create a space charge layer depleted of electrons and negatively charged oxygen ions on the surface. It has been reported elsewhere that doping of TiO<sub>2</sub> with Fe increases the oxidation activity of the oxide and this has been related to a higher density of oxygen vacancies [22]. As the metal oxides approach to stoichiometry, however, oxygen vacancies are reduced and the conductivity of the oxide becomes extremely low (high resistance) and gas-sensing measurements becomes difficult.

In this paper pure and Fe-doped nanostructured tungsten oxide thin films with small Fe concentrations were studied for low temperature NO<sub>2</sub> gas sensing. Most of the metal oxide gas sensors that have been investigated today are not sufficiently sensitive at lower temperatures (<150 °C) and must be thermally-activated at elevated temperature (>250 °C). The high operating temperature leads to a long term material stability problem due to diffusion and sintering effects of the sensors and also demand higher power consumption [23]. This makes them unsuitable for battery operated sensing that would be advantageous in some in situ applications. Thus it is desirable to develop sensors with enhanced sensing characteristics at lower operating temperature, which is the main focus of this paper. DC reactive sputtering was used to produce pure and Fe-doped tungsten oxide films. Different concentrations of Fe were achieved by varying the sputtering power of the Fe-target. The properties of tungsten oxide films with small concentrations of Fe developed by sputtering for gas sensing applications are not well documented in the literature [24]. Since Fe has a similar atomic radius (0.64 nm) to W (0.62 nm), it can be introduced in small quantities as a substitutional impurity in the WO<sub>3</sub> crystal structure. This can produce crystal distortions that can influence the physical, chemical, electronic, optical and gas sensing properties of the material. The microstructure, composition, crystallinity and morphology of the films were analyzed using atomic force microscope (AFM), X-ray photoelectron spectroscopy (XPS) and Raman Spectroscopy. The optical properties of the films were characterized with UV-Vis-NIR spectrophotometer. The thickness and surface roughness of the films were determined using Ellipsometer and their results were confirmed using Mechanical Stylus Profilometer. Gas sensing measurements towards NO<sub>2</sub> of different concentrations (1–12 ppm) at different operating temperatures (100–300 °C) were carried out in an 1100 cc volume test chamber using a flow through method. From the measurements different sensing parameters (response amplitude (i.e. sensitivity), response and recovery times) were determined and the performance of the sensors have been evaluated.

## 2. Experimental methods

### 2.1. Sample preparation

DC confocal magnetron sputtering (PVD 75 K.J. Lesker) was used to produce Fe-doped tungsten oxide thin films. The PVD has four

targets that enable to co-sputtering more than two materials simultaneously using independent power supply. A 50 mm diameter W (99.95% purity) and Fe (99.9% purity) targets were used as source materials and oxygen was introduced as a reactive gas. After the chamber was evacuated to a base pressure of about  $5.3 \times 10^{-6}$  Pa, then Ar was introduced and maintain at a partial pressure of 1.60 Pa during sputtering. The argon-to-oxygen ratio in the chamber was kept to 4:1, respectively. The films with various concentrations of Fe have been deposited on unheated (24 °C room temperature) microscope glass and 8 mm × 8 mm alumina substrates. The alumina electrodes had a pre-printed Pt-interdigitated fingers consisting of line width 100 μm and height 300 nm and were used for gas sensing measurements. A 40 W power on the tungsten target and 0, 5, 20 and 40 W on the Fe target have been applied to vary the composition of the films. To ensure film uniformity, the substrate holder was allowed to rotate at 10 rpm. All the samples were sputtered for 80 min including a pre-sputtering period of 5 min to remove any contaminants. Four different samples were produced using the input parameters shown in Table 1. The names of the samples are given based on the Fe-concentrations obtained from XPS measurements.

### 2.2. Film characterization

Film thickness measurements were performed using M-2000 Ellipsometer (J. A. Woollam Co., Inc.) and the results were confirmed with mechanical stylus profilometer (Bruker Dektak XT) using a 2 μm tip. To observe the surface features of the films, AFM morphology and phase scans were performed using Nanoscope III AFM (model K-A102006344) with nominal tip diameter of 10 nm operated in tapping mode using Si cantilever. The concentration of Fe in WO<sub>3</sub> film was obtained from XPS survey spectra over the binding energy range of 0–1200 eV. The XPS data was acquired using a Kratos Axis ULTRA XPS incorporating a 165 mm hemispherical electron energy analyser. The incident radiation was monochromatic Al Kα X-rays (1486.6 eV) at 150 W (15 kV, 10 mA) and at 45° to the sample surface. Photoelectron data was collected at a take-off angle of theta = 90°. Survey (wide) scans were taken at analyser pass energy of 160 eV.

Raman measurements were performed using a Renishaw inVia Raman spectrometer to determine the chemical structure and physical state of the films. A Renishaw frequency doubled NdYAG laser excitation source of wavelength 532 nm was used. To avoid local heating of the samples, a low power of about 5 mW was applied on the samples. A Raman shift between the wavenumbers 200–1200 cm<sup>-1</sup> has been measured. The transmittance of the films on glass substrates was measured using Cary 50 UV-Vis-NIR spectrophotometer. The measurements were performed in the wavelength range 300–1100 nm at a normal angle of incidence.

### 2.3. Gas sensing measurements

Gas sensing measurements towards NO<sub>2</sub> were carried out using a flow through method using a high precision multi-channel gas testing system, including a 1100 cc volume test chamber capable of testing four sensors in parallel, 8 high precision mass flow controllers (MKS 1479A) to regulate the gas mixture, 8 channel MFC processing unit (MKS 647C), a pico-ammeter (Keithley 6487)

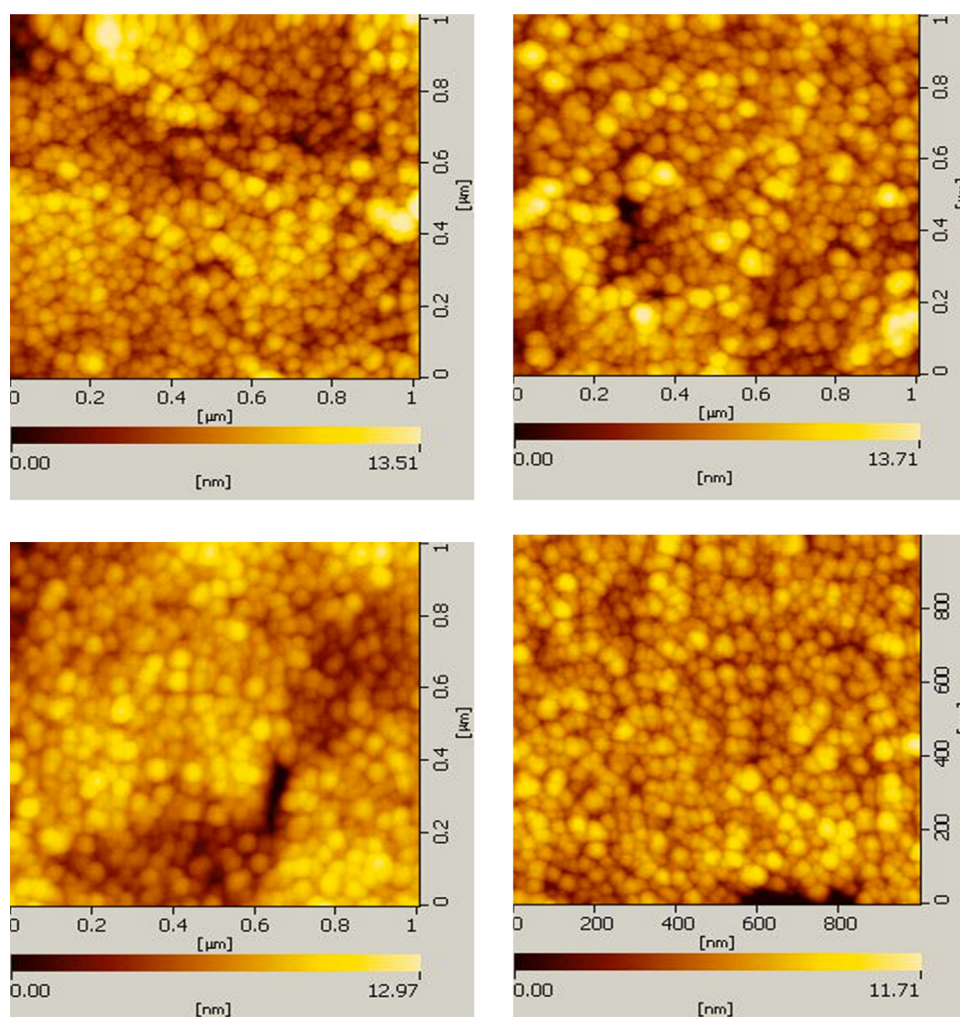


**Fig. 1.** AFM morphology of (a) pure tungsten oxide film and (b–d) Fe-doped tungsten oxide films (0.03, 1.33, 2.6 at%, respectively) obtained using tapping mode.

and a climatic chamber to control the temperature. The measurements were performed between 100 and 300 °C with a mixture of synthetic air and NO<sub>2</sub> target gas of different concentrations (1–12 ppm). The concentration range has been selected within the threshold limit values acceptable in various applications [20]. The right concentration of gases in air was obtained by adjusting the respective flow rates via the MFCs, while maintaining a total constant flow rate of 200 sccm (mL/min). The response upon gas exposure was evaluated by measuring the sensors resistance variation with bias voltage of 1 V. The temperature range of 100–300 °C was regulated by applying voltage to a micro-ceramic heating element having resistance of 44 Ω (Sakaguchi MS-3).

The gas exposure duration for each measurement was 5 min. A reasonable 20 min time was allowed for the recovery of the sensors after switching off the target gas prior to the next exposure. The sensor response amplitude or sensitivity ( $S$ ) is used as the measure of the sensor response and is defined to be a positive quantity and for oxidizing gases such as NO<sub>2</sub>:

$$S = \frac{R - R_{\text{air}}}{R_{\text{air}}} = \frac{\Delta R}{R_{\text{air}}} \quad (1)$$

where  $R_{\text{air}}$  is the steady state resistance value in the reference air and  $R$  the final resistance of the sensor when exposed to the target gas achieved within a reasonable time (5 min) [25]. The response was determined by considering the time required for the sensor to reach 90% of the final  $S$  value after exposed to the target gas.

Similarly the recovery time of the sensor was also obtained from the time the sensor requires to recover the 90% of the maximum  $S$  value so it reached 10% above the baseline resistance after switching off the target gas.

### 3. Results and discussion

Table 2 shows post-deposition values of the pure and Fe-doped tungsten oxide films on glass substrate obtained using Ellipsometer. The thickness of the different films ranges between 155 and 186 nm. From the results the deposition rate of the pure film (2.5 nm/min) was found to be slightly higher than the Fe-doped films (2.2 nm/min). All the films on glass substrate have shown similar surface roughness between 8 and 10 nm. The film thickness and surface roughness values measured by Ellipsometer were comparable to the results obtained using mechanical stylus profiler.

**Table 2**

Post-deposition values of pure and Fe-doped tungsten oxide films on glass substrate obtained using Ellipsometer.

| Specimen                       | Film thickness (nm) | Surface roughness (nm) | Deposition rate (nm/min) |
|--------------------------------|---------------------|------------------------|--------------------------|
| Pure WO <sub>3</sub>           | 186                 | 12                     | 2.5                      |
| WO <sub>3</sub> :Fe (0.03 at%) | 155                 | 8                      | 2.1                      |
| WO <sub>3</sub> :Fe (1.33 at%) | 168                 | 11                     | 2.2                      |
| WO <sub>3</sub> :Fe (2.6 at%)  | 165                 | 10                     | 2.2                      |



**Table 3**

Surface roughness ( $R_a$ ) and grain size ( $D$ ) of pure and Fe-doped films obtained using AFM. The films have been scanned over small area ( $1\ \mu\text{m} \times 1\ \mu\text{m}$ ) on the alumina and Pt regions of the electrodes.

| Specimen                           | $R_a$ on alumina (nm) | $D$ on alumina (nm) | $R_a$ on Pt (nm) | $D$ on Pt (nm) |
|------------------------------------|-----------------------|---------------------|------------------|----------------|
| Pure $\text{WO}_3$                 | 1.64                  | 43.0                | 1.53             | 45.0           |
| $\text{WO}_3:\text{Fe}$ (0.03 at%) | 1.53                  | 47.8                | 1.6              | 49.5           |
| $\text{WO}_3:\text{Fe}$ (1.33 at%) | 1.49                  | 50.4                | 1.62             | 51.6           |
| $\text{WO}_3:\text{Fe}$ (2.6 at%)  | 1.78                  | 57.2                | 1.37             | 54.4           |

Fig. 1a–d shows AFM morphologies of the pure and Fe-doped tungsten oxide films on alumina substrate obtained using tapping mode. From the images the morphologies of the different samples (Fig. 1(a): pure film; (b): 0.3 at% Fe; (c): 1.33 at% Fe; (d): 2.6 at% Fe) appeared similar with narrow grain size distribution between 43 and 57 nm and surface roughness less than 2 nm. The median grain size of the films was about 50 nm and from theoretical study the smaller size grains can significantly enhanced sensor response [10]. From AFM images analysis, a relatively larger grain size in the film with the highest Fe-doping (2.6 at% Fe) was obtained compared to the other films as shown in Table 3. Various AFM images were scanned at the different area of the electrodes to investigate the effect of the under-layer material (alumina or Pt) on the surface roughness and grain size. From the investigation, all the films on the Pt interdigitated surface have shown similar roughness and grain size with those films grown between the Pt fingers (i.e. on alumina surface) as shown in Table 3. However, larger film defects were observed in the alumina region of the sensor compared to the film defects on Pt fingers. The results can be observed from the AFM morphology in Fig. 2 obtained at the Pt and alumina interface. This finding may be useful for future design of sensor electrodes as defects have significant effect to sensor performance. It is to be noted that the images shown in Fig. 1 above are all for the films

on the alumina surface. Fig. 2 also shows a clear boundary at the Pt and alumina interface. As the thickness of the Pt interdigitated electrode is 300 nm and the thickness of the films is about 170 nm, there may be some portion of the Pt thickness not covered by the film. However, the influence of the bulk Pt electrode on gas sensing may be negligible compared to the high surface area obtained from the nanoparticles of the films. Fig. 3 shows AFM scans of the pure and Fe-doped (2.6 at%) samples over larger area ( $5\ \mu\text{m} \times 5\ \mu\text{m}$ ). The AFM images indicated protrusion of individual grains randomly distributed throughout the film. From the figure shorter spacing and more evenly grown spikes appeared in the Fe-doped films with average height of about 50 nm. These features are more beneficial for gas sensing compared to that of the pure film.

Raman spectroscopy has been employed to analyze the chemical and crystalline nature of the films as there was no diffraction observed from XRD grazing incidence measurement. Fig. 4 shows normalized Raman spectra of tungsten oxide films in the wavenumber regime between 200 and  $1200\ \text{cm}^{-1}$ . From the figure bands in the range of  $550\text{--}1050\ \text{cm}^{-1}$  associated to the W–O stretching modes can be observed. There was no obvious peak detected in the established bending mode wavenumber of  $200\text{--}550\ \text{cm}^{-1}$ . The weak and broad bands centred at about  $951\ \text{cm}^{-1}$  and  $752\ \text{cm}^{-1}$  features some amorphous characteristic of the tungsten oxide films.

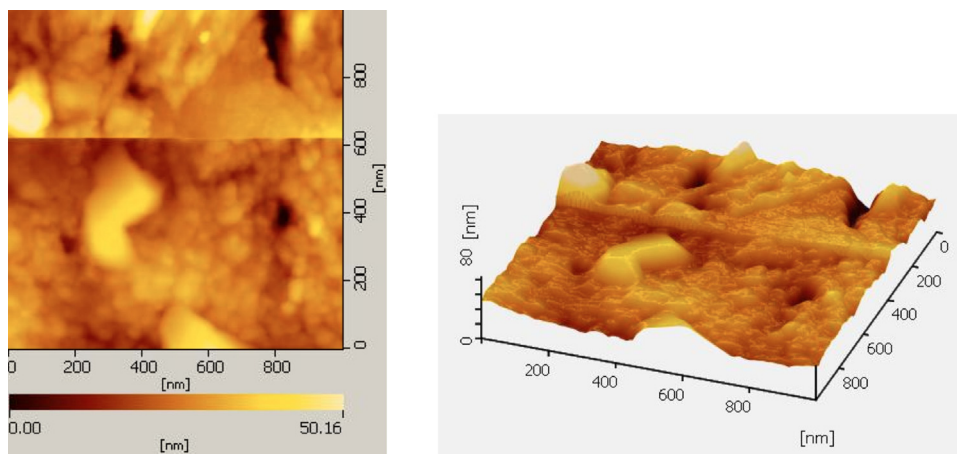


**Fig. 2.** AFM 2D and 3D images of  $\text{WO}_3:\text{Fe}$  2.6 at% film at the Pt–alumina interface. Inset shows film on (1) alumina region and (2) Pt area.

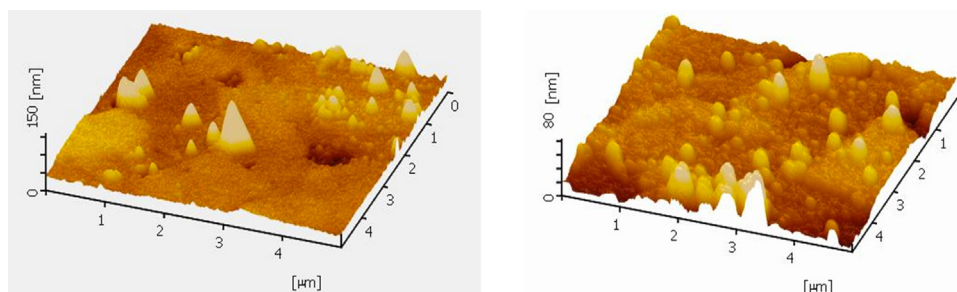


**Fig. 3.** AFM morphology of (a) pure film and (b) 2.6 at% Fe-doped film that have been scanned over larger area ( $5\ \mu\text{m} \times 5\ \mu\text{m}$ ) of the samples. The images were obtained using tapping mode.

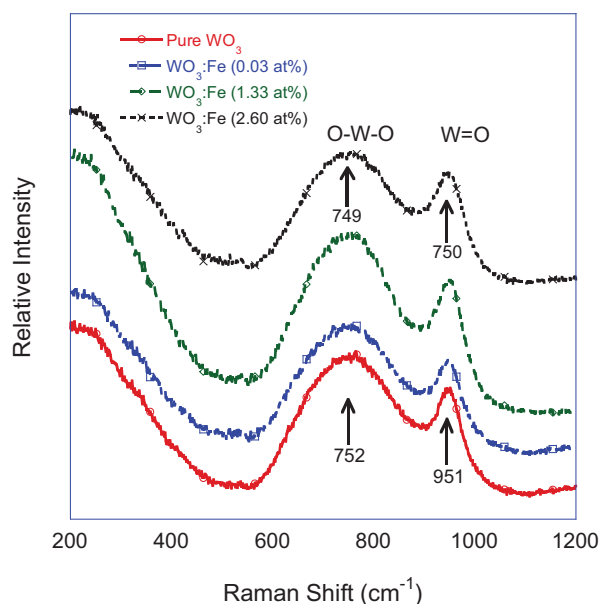
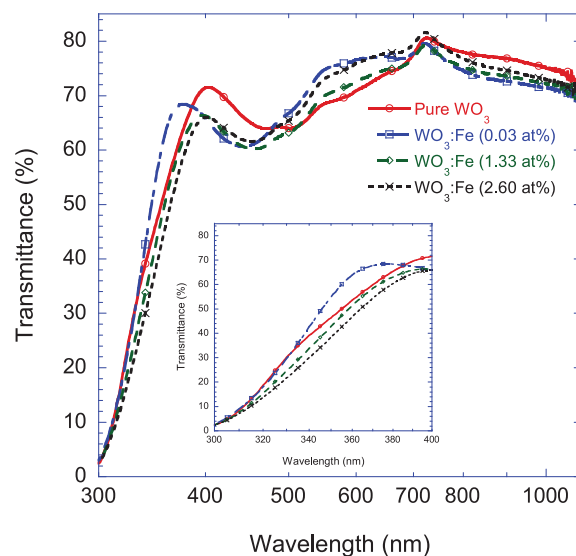
**Table 4**Atomic concentration of Fe in WO<sub>3</sub> films obtained using XPS after 2 min etching using Ar.

| Specimen                       | Nominal Composition | W at% | O at% | Fe at% | C at% | Na at% |
|--------------------------------|---------------------|-------|-------|--------|-------|--------|
| Pure WO <sub>3</sub>           | WO <sub>3</sub>     | 37.51 | 60.7  | –      | –     | 1.79   |
| WO <sub>3</sub> :Fe (0.03 at%) | WO <sub>3</sub> :Fe | 37.04 | 60.81 | 0.03   | –     | 2.12   |
| WO <sub>3</sub> :Fe (1.33 at%) | WO <sub>3</sub> :Fe | 35.97 | 60.9  | 1.33   | –     | 1.80   |
| WO <sub>3</sub> :Fe (2.6 at%)  | WO <sub>3</sub> :Fe | 34.42 | 59.25 | 2.60   | 2.67  | 1.06   |

These peak frequencies are usually assigned in the literature to the stretching frequency modes O–W–O and bridging oxygen W=O [1]. Amorphous and nanostructured tungsten oxide films are usually composed of O–W–O mode, similar to the WO<sub>6</sub> octahedral structure of the bulk crystal, with terminal W=O at the surface and grain boundaries of the films [26]. The peak position of the W=O was nearly unchanged (951 cm<sup>−1</sup>) whereas the position of the low frequency O–W–O mode was shifted to lower frequency by only 3 cm<sup>−1</sup> when the pure film was doped with Fe. Although this shift may not be sufficient to observe a significant variation in the chemical properties of the two kinds of films but the ratio of the integrated Raman intensity of W=O to O–W–O bands appeared to increase with increasing Fe concentrations and this indicated an increase in the number of defects.

The composition of the films on the surface was obtained from XPS general survey spectra on glass substrate. From the spectra, peaks of W, O, Na and C were observed in all of the films and Fe in those co-sputtered films. The Na is most likely obtained from the glass substrate after annealing at 300 °C and was higher in the film with 5 W sputtering power for Fe. The carbon is most likely from the atmosphere and was removed or significantly reduced after 2 min of etching the films. From XPS high resolution spectra the amount of Fe in the WO<sub>3</sub> films was quantified as 0.03, 1.33 and 2.6 at% for the samples sputtered at 5, 20 and 40 W of power, respectively (Table 4). Practically very small Fe was detected in the sample sputtered using 5 W and such value can be within the instruments marginal error. This indicates that the 5 W power was not sufficient to sputter deposit Fe onto the substrate.

The optical properties of the pure and Fe-doped tungsten oxide films were measured in the solar wavelength range between 300 nm and 1100. From Fig. 5 sharp absorption edge of the films

**Fig. 4.** Raman spectra of pure and Fe-doped tungsten oxide films in the wavenumber regime between 200 and 1200 cm<sup>−1</sup>.**Fig. 5.** Transmittance of pure and Fe-doped tungsten oxide films as a function of wavelength between 300 and 1100 nm. Inset shows spectra in the wavelength 300–400 nm.

can be observed below 400 nm. The on-set of the absorption edge for the Fe-doped films appeared to be slightly shifted (see inset in Fig. 5 for better resolution) to longer wavelength (red shift) with increasing Fe concentrations. It is hypothesized that Fe with atomic radius of 0.64 nm can be introduced in small quantities as a substitutional impurity as it has similar size to W (0.62 nm) and this can cause distortion in the WO<sub>3</sub> crystal structure. Such lattice mismatch combined with the properties of the film and the type of strain (tensile or compressive) induced into the film during sputtering can produce either blue or red shift in the optical absorption. Due to the nature of the sputter deposition, compressive strain would be expected in the films and this would result a red shift in the optical absorption which would also influence the optical bandgap energy of the films [27]. In order to see such effect on the band gap, first the visible transmittance of the films was calculated by weighting the spectral transmittance of the films to the intensity of the corresponding visible spectrum for air mass 1.5. From the calculation, the pure and Fe doped tungsten oxide films were found to be fairly transparent, having visible transmittance in excess of 70% as shown in Table 5. The optical band gaps ( $E_g$ ) of the various films were evaluated from the transmittance spectra (Fig. 5) by plotting  $(\alpha h\nu)^{1/2}$  vs  $h\nu$  that is appropriate for an indirect band gap material and then using linear extrapolation to the energy axis ( $\alpha = 0$ ) [28]. The optical

**Table 5**Film thickness ( $d$ ), visible transmittance ( $T_{vis}$ ) and optical band gap ( $E_g$ ) of pure and Fe-doped tungsten oxide films deposited on glass substrate.

| Specimen                       | $d$ (nm) | $T_{vis}$ (%) | $E_g$ (eV) |
|--------------------------------|----------|---------------|------------|
| Pure WO <sub>3</sub>           | 186      | 72            | 3.30       |
| WO <sub>3</sub> :Fe (0.03 at%) | 155      | 73            | 3.25       |
| WO <sub>3</sub> :Fe (1.33 at%) | 168      | 71            | 3.20       |
| WO <sub>3</sub> :Fe (2.6 at%)  | 165      | 73            | 3.15       |

absorption coefficient ( $\alpha$ ) at incident photon energy ( $h\nu$ ) is obtained using the relationship:

$$\alpha d = \ln \left( \frac{1}{T_{vis}} \right) \quad (2)$$

where  $d$  and  $T_{vis}$  are the thickness and visible transmittance of the films, respectively (see Table 5). From Table 5, there is a slight decrease in the optical band gap when Fe was incorporate into the tungsten oxide film [29]. The red shift observed in the optical absorption caused a negative shift (reduction) in the bandgap of the  $WO_3$  film. The optical band gap of the Fe-doped tungsten oxide films deposited by sputtering is not readily available in the literature for comparison. However, the values obtained here are found to be within the ranges of optical band gap of the Fe-doped films obtained by e-beam evaporation as reported elsewhere [30].

The sensing characteristics of the pure and Fe-doped  $WO_3$  films towards 1 to 12 ppm of  $NO_2$  gas at different working temperatures (100–300 °C) were measured. The response amplitude (i.e. sensitivity) of the sensors has been quantified using Eq. (1) and the results are shown in Figs. 6 and 7a–d. From the results, all the sensors have shown noticeable response above 3 ppm. At the operating temperature of 100 °C (Fig. 6), the response amplitude (sensitivity) of the pure  $WO_3$  film has been improved after Fe-doping but with very slow dynamics and hence. When the working temperature was increased to 150 °C, only the 2.6 at% Fe-doped film has shown high sensitivity and reasonable response dynamics (see Fig. 7a). All the other films (pure, 0.03 at% Fe and 1.33 at% Fe) have shown acceptable response only above 200 °C as shown in Fig. 7b (0.03 at% Fe), c (1.33 at% Fe) and d (pure film). Due to the very slow response

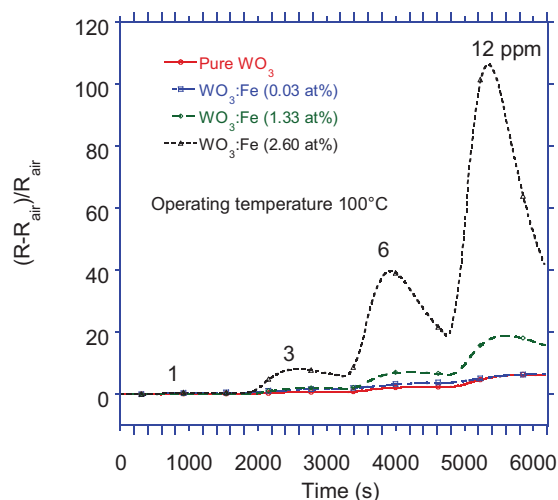


Fig. 6. Dynamic response of pure and Fe-doped  $WO_3$  sensors towards various concentrations of  $NO_2$  gas (1–12 ppm) measured at 100 °C.

and recovery times of these films (pure, 0.03 at% Fe and 1.33 at% Fe) below 200 °C, no further analysis has been reported at 150 °C and 100 °C. From Fig. 8a, it can be observed that the response amplitude (sensitivity) of all the sensors declined with increasing temperature. This shows that while the sensitive of the films is higher at lower temperatures, great focus should be given on how to improve the slow dynamics. From the optical measurements, the band gap of

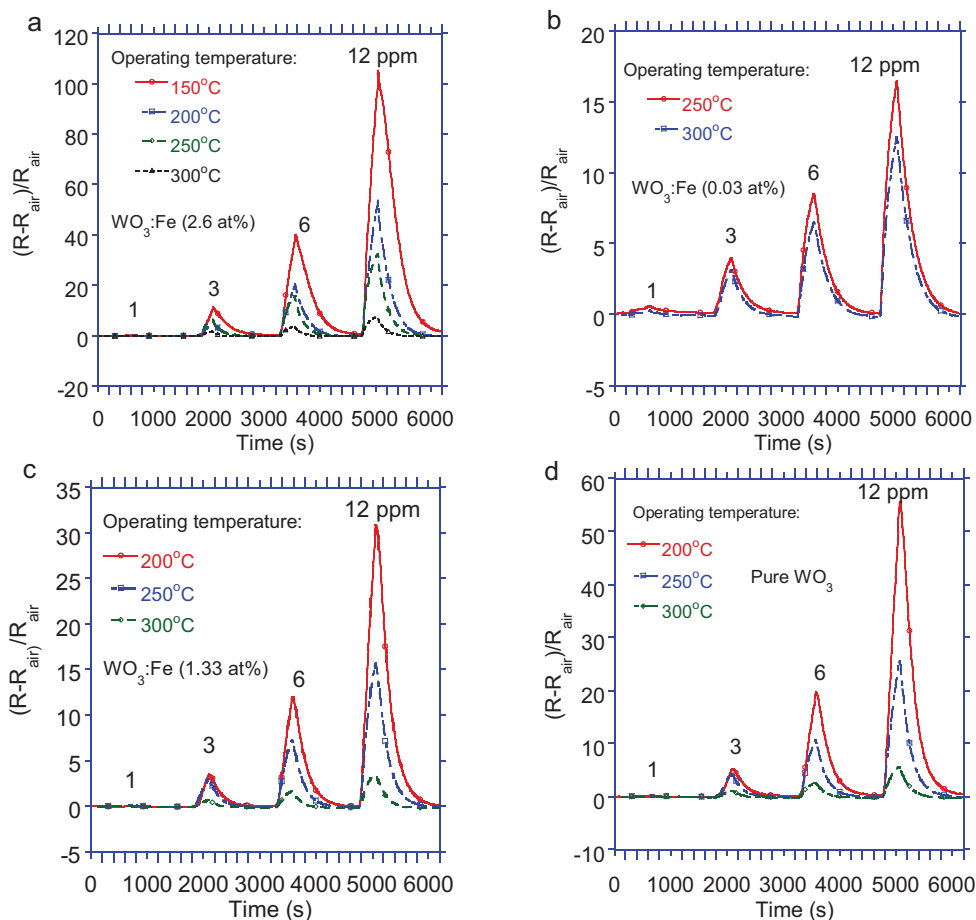
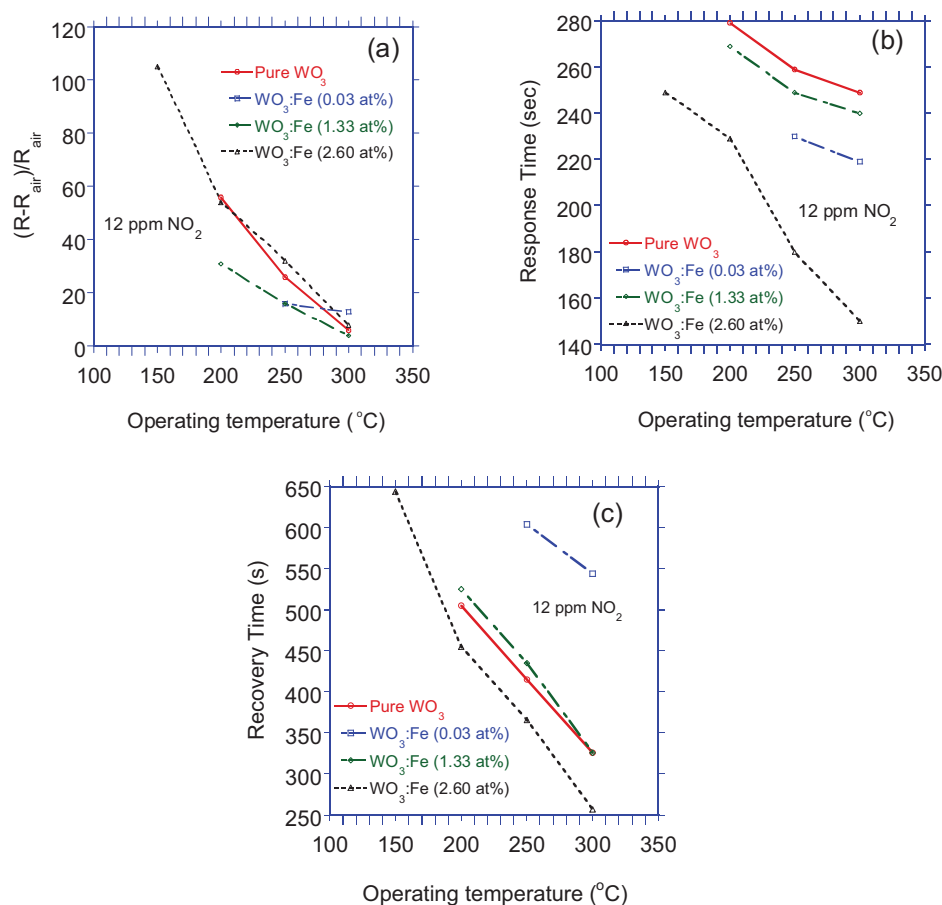


Fig. 7. Dynamic response of different Fe-doped  $WO_3$  films (a) 2.6 at% Fe, (b) 0.03 at% Fe, (c) 1.33 at% Fe as compared to (d) pure  $WO_3$  film towards various concentrations of  $NO_2$  gas (1–12 ppm) measured between 150 and 300 °C.



**Fig. 8.** (a) Response amplitude (i.e. sensitivity), (b) response time, and (c) recovery time of pure and Fe-doped WO<sub>3</sub> films towards 12 ppm NO<sub>2</sub> gas at various working temperatures between 150 and 300 °C.

the pure film has been reduced by 0.15 eV after doped with 2.6 at% Fe, and this makes gas sensing measurements at lower temperature (150 °C) easier due to reduced resistivity and especially, when the pure film exhibits a very high resistance.

Fig. 8b, c shows response and recovery times of the pure and Fe-doped WO<sub>3</sub> films towards 12 ppm NO<sub>2</sub> gas between 150 and 300 °C. The sample with 0.03 at% Fe has the slowest recovery time and its response amplitude deviated from the other films. The sputtering power of Fe in the sample was only 5 W and as a result very little Fe was detected by XPS which indicated that the power used was not sufficient to sputter deposit the material and consequently the gas sensing properties of the film appeared different compared to the other films. From the results shown in Fig. 8a, the response amplitude of the 2.6 at% Fe-doped film became comparable to that of the pure film at operating temperature of 200 °C and yet with faster dynamics. The best sensing parameters were achieved from the 2.6 at% Fe sensor at operating temperature of 150 °C. The response amplitude (sensitivity), response and recovery times of the sensor towards 12 ppm NO<sub>2</sub> gas at 150 °C were 105, 250 s and 650 s, respectively.

Previous work of e-beam evaporated Fe-doped WO<sub>3</sub> with higher concentration (10 at% Fe) also showed a lower working temperature (150 °C) but longer response and recovery times, mainly due to reduced film porosity [24]. Film thickness also can play a significant role in improving sensing parameters and from previous work on e-beam evaporated Fe-doped WO<sub>3</sub> films with different thicknesses (100–500 nm), the 400 nm sensor has shown the best response and recovery times [24]. In this work, the thicknesses of the different films (155–186 nm) and Fe concentrations (0–2.6 at% Fe) were not optimized. From Raman it is found that the number

of defects appeared to increase with increasing Fe concentrations which are useful for enhanced gas sensing at lower temperatures. From the above results, the 2.6 at% Fe-doped WO<sub>3</sub> film has the lowest operating temperature (150 °C) with acceptable dynamics and this can be due to the lower optical band gap and higher number of defects. From Fig. 6, the sensitive of the 2.6 at% Fe film at 100 °C is very significant but the slow response and recovery times should be improved in order to see its feasibility in practical application. Thus further investigation of the tungsten oxide films with several samples by varying various sputter deposition conditions (power, pressure, Fe-concentrations, film thickness) should be applied for maximizing gas sensing parameters (response amplitude, response and recovery times and operating temperature).

#### 4. Conclusions

DC reactive sputtering was used to deposit Fe-doped tungsten oxide thin films of small concentrations (0–2.6 at% Fe) at room temperature and the films were subsequently annealed at 300 °C for 1 h in air. The different films have thickness between 155 and 186 nm and grain size between 43 and 57 nm. Higher amount of defects were observed in the films grown on the alumina area of the samples compared to the films grown on the Pt interdigitated electrode surface but with similar roughness (<2 μm). This finding can be useful for optimizing sensor electrodes as defects have significant effect on sensing performance. From Raman spectrum broader peaks with typical characteristics of partially crystallized films were observed. With increasing Fe concentration, the ratio of the integrated Raman intensity of W=O to O–W–O bands increases



and thus an increase in the number of defects. The visible transmittance of all the films remained similar (>70%) but their optical band gap decreased with increasing Fe concentration from 3.30 to 3.15 eV. Since Fe has slight higher atomic radius (0.64 nm) than W (0.62 nm), it can distort the crystal structure of the  $\text{WO}_3$  and thereby reduced the optical band gap of the film. The response amplitude of the  $\text{WO}_3$  film with 2.6 at% Fe was found to be significantly higher and stable towards 3–12 ppm  $\text{NO}_2$  gas with reasonable dynamics at operating temperature of 150 °C. The other films have only shown acceptable response above 200 °C. From the overall results, enhanced  $\text{NO}_2$  gas sensing at lower operating temperature (150 °C) was achieved from tungsten oxide film doped with 2.6 at% Fe and this is concluded due to the decrease in the optical band gap and an increase in the number of defects.

## Acknowledgments

This work has been supported by ATN-DAAD Joint Research Cooperation Scheme and JSPS. Dr. Torsten Gerling (Leibniz-Institute for Plasma Science and Technology, Germany) is acknowledged for his contribution on film deposition and Dr. Barry Wood (University of Queensland, Australia) for XPS data acquisition. AFM characterization has been made at the Laboratory of Nanoscience and Materials at Hokkaido University (Japan). This research was mainly done at IFE Central Analytical Research Facility at QUT.

## References

- [1] L.J. LeGore, R.J. Lad, S.C. Moulzolf, J.F. Vetelino, B.G. Frederick, E.A. Kenik, Defects and morphology of tungsten trioxide thin films, *Thin Solid Films* 406 (2002) 79–86.
- [2] C. Cantalini, H.T. Sun, M. Faccio, M. Pelino, S. Santucci, L. Lozzi, M. Passacantando,  $\text{NO}_2$  sensitivity of  $\text{WO}_3$  thin film obtained by high vacuum thermal evaporation, *Sens. Actuators B* 31 (1996) 81–87.
- [3] R. Sivakumar, M. Jayachandran, C. Sanjeeviraja, Studies on the effect of substrate temperature on (VI–VI) textured tungsten oxide ( $\text{WO}_3$ ) thin films on glass,  $\text{SnO}_2$ :F substrates by PVD:EBE technique for electrochromic devices, *Mater. Chem. Phys.* 87 (2004) 439–445.
- [4] T. Siciliano, A. Tepore, G. Micocci, A. Serra, D. Manno, E. Filippo,  $\text{WO}_3$  gas sensors prepared by thermal oxidization of tungsten, *Sens. Actuators B: Chem.* 133 (2008) 321–326.
- [5] Y.-G. Choi, G. Sakai, K. Shimanoe, N. Miura, N. Yamazoe, Wet process-prepared thick films of  $\text{WO}_3$  for  $\text{NO}_2$  sensing, *Sens. Actuators B* 95 (2003) 258–265.
- [6] A. Hoel, L.F. Reyes, P. Hesler, V. Lantto, C.G. Granqvist, Nanomaterials for environmental applications: novel  $\text{WO}_3$ -based gas sensors made by advanced gas deposition, *Curr. Appl. Phys.* 4 (2004) 547–553.
- [7] S.-K. Song, J.-S. Cho, W.-K. Choi, H.-J. Jung, D. Choi, J.-Y. Lee, H.-K. Baik, S.-K. Koh, Structure and gas-sensing characteristics of undoped tin oxide thin films fabricated by ion-assisted deposition, *Sens. Actuators B* 46 (1998) 42–49.
- [8] S.C. Moulzolf, S.-A. Ding, R.J. Lad, Stoichiometry and microstructure effects on tungsten oxide chemiresistive films, *Sens. Actuators B: Chem.* 77 (2001) 375–382.
- [9] A. Rothschild, Y. Komem, The effect of grain size on the sensitivity of nanocrystalline metal-oxide gas sensors, *J. Appl. Phys.* 95 (2004) 6374–6380.
- [10] X. Wang, S.S. Yee, W.P. Carey, Transition between neck-controlled and grain-boundary-controlled sensitivity of metal-oxide gas sensors, *Sens. Actuators B: Chem.* 25 (1995) 454–457.
- [11] G. Korotcenkov, V. Brinzari, A. Cerneavski, M. Ivanov, V. Golovanov, A. Cornet, J. Morante, A. Cabot, J. Arbiol, The influence of film structure on  $\text{In}_2\text{O}_3$  gas response, *Thin Solid Films* 460 (2004) 315–323.
- [12] R. Artzi-Gerlitz, K.D. Benkstein, D.L. Lahr, J.L. Hertz, C.B. Montgomery, J.E. Bonevich, S. Semancik, M.J. Tarlov, Fabrication and gas sensing performance of parallel assemblies of metal oxide nanotubes supported by porous aluminum oxide membranes, *Sens. Actuators B: Chem.* 136 (2009) 257–264.
- [13] H. Kawasaki, T. Ueda, Y. Suda, T. Ohshima, Properties of metal doped tungsten oxide thin films for  $\text{NO}_x$  gas sensors grown by PLD method combined with sputtering process, *Sens. Actuators B: Chem.* 100 (2004) 266–269.
- [14] V. Khatko, E. Llobet, X. Vilanova, J. Brezmes, J. Hubalek, K. Malysz, X. Correig, Gas sensing properties of nanoparticle indium-doped  $\text{WO}_3$  thick films, *Sens. Actuators B: Chem.* 111–112 (2005) 45–51.
- [15] M.A. Ponce, C.M. Aldao, M.S. Castro, Influence of particle size on the conductance of  $\text{SnO}_2$  thick films, *J. Eur. Ceram. Soc.* 23 (2003) 2105–2111.
- [16] J. Shieh, H.M. Feng, M.H. Hon, H.Y. Juang,  $\text{WO}_3$  and W–Ti–O thin-film gas sensors prepared by sol–gel dip-coating, *Sens. Actuators B: Chem.* 86 (2002) 75–80.
- [17] A. Rothschild, F. Edelman, Y. Komem, F. Cosandey, Sensing behavior of  $\text{TiO}_2$  thin films exposed to air at low temperatures, *Sens. Actuators B: Chem.* 67 (2000) 282–289.
- [18] D.H. Yoon, G.M. Choi, Microstructure and CO gas sensing properties of porous  $\text{ZnO}$  produced by starch addition, *Sens. Actuators B: Chem.* 45 (1997) 251–257.
- [19] A. Boudiba, C. Zhang, C. Navio, C. Bittencourt, R. Snyders, M. Debliquy, Preparation of highly selective, sensitive and stable hydrogen sensors based on Pd-doped tungsten trioxide, *Procedia Eng.* 5 (2010) 180–183.
- [20] M. Stankova, X. Vilanova, J. Calderer, E. Llobet, J. Brezmes, I. Gràcia, C. Cané, X. Correig, Sensitivity and selectivity improvement of rf sputtered  $\text{WO}_3$  microhotplate gas sensors, *Sens. Actuators B: Chem.* 113 (2006) 241–248.
- [21] E. Rossinyol, A. Prim, E. Pellicer, J. Rodríguez, F. Peiró, A. Cornet, J.R. Morante, B. Tian, T. Bo, D. Zhao, Mesoporous pure and copper-catalyzed tungsten oxide for  $\text{NO}_2$  detection, *Sens. Actuators B: Chem.* 126 (2007) 18–23.
- [22] A. Roldan, M. Boronat, A. Corma, F. Illas, Theoretical confirmation of the enhanced facility to increase oxygen vacancy concentration in  $\text{TiO}_2$  by iron doping, *J. Phys. Chem. C* 114 (2010) 6511–6517.
- [23] T.A. Kunt, T.J. McAvoy, R.E. Cavicchi, S. Semancik, Optimization of temperature programmed sensing for gas identification using micro-hotplate sensors, *Sens. Actuators B: Chem.* 53 (1998) 24–43.
- [24] T. Tesfamichael, A. Ponzoni, M. Ahsan, G. Faglia, Gas sensing characteristics of Fe-doped tungsten oxide thin films, *Sens. Actuators B: Chem.* 168 (2012) 345–353.
- [25] O. Berger, T. Hoffmann, W.-J. Fischer, V. Melev, Tungsten-oxide thin films as novel materials with high sensitivity and selectivity to  $\text{NO}_2$ ,  $\text{O}_3$ , and  $\text{H}_2\text{S}$ . Part II: application as gas sensors, *J. Mater. Sci.: Mater. Electron.* 15 (2004) 483–493.
- [26] A. Baserga, V. Russo, F. Di Fonzo, A. Bailini, D. Cattaneo, C.S. Casari, A. Li Bassi, C.E. Bottani, Nanostructured tungsten oxide with controlled properties: synthesis and Raman characterization, *Thin Solid Films* 515 (2007) 6465–6469.
- [27] S. Bandyopadhyay, *Physics of Nanostructured Solid State Devices*, Springer, New York, 2012.
- [28] J. Tauc, *Amorphous and Liquid Semiconductors*, Plenum Press, London, 1974.
- [29] A.Z. Moshfegh, R. Azimird, O. Akhavan, Optical properties and surface morphology of evaporated  $\text{WO}_3$ – $\text{Fe}_2\text{O}_3$  thin films, *Thin Solid Films* 484 (2005) 124–131.
- [30] T. Tesfamichael, M. Arita, T. Bostrom, J. Bell, Thin film deposition and characterization of pure and iron-doped electron-beam evaporated tungsten oxide for gas sensors, *Thin Solid Films* 518 (2010) 4791–4797.

## Biographies

**Tuquabo Tesfamichael** received his Ph.D. in Solid State Physics in 2000 from Uppsala University, Sweden. Earlier degrees include Swedish Licentiate Degree in Materials Physics from Uppsala University (1998) and B.Sc. in Physics from University of Asmara, Eritrea (1989). He has been academic teaching and research staff at Queensland University of Technology since 2001. Dr. Tesfamichael's research interest has been focused towards better understanding and development of nanomaterials, thin film coatings, and surface engineering for solar energy, gas sensors, plasma medicine and antibacterial treatments. He has published over 40 referred articles in high impact and widely read journals.

**Carlo Piloto** is a Ph.D. student at Queensland University of Technology. He received his master degree in Telecommunication Engineer (2004) from University of Padua (Italy) and had been working for multinational semiconductor company for seven years. His Ph.D. is focused on development of gas sensors based on carbon nanomaterials, thin films metal oxides and hybrid carbon–metal oxide thin films. His research emphasis is into lowering operating temperature of gas sensors for better portability into field applications. He has recently published a paper on the synthesis of caesium doped graphene oxide and its application to the development of a novel  $\text{NO}_2$  gas sensor.

**Masashi Arita** had received his Ph.D. in September 1987 from Swiss Federal Institute of Technology Zurich and then worked as Senior Researcher at the International Research Laboratory, Ciba-Geigy Japan Ltd. In June 1990, he held a Lecturer position at Nagoya University (Japan) teaching physics, mathematics and materials engineering and researching on materials science. In April 1997 he became Associate Professor at School of Engineering, Hokkaido University (Japan) and teaching physics, informatics and materials science, and researching on quantum transport of magnetic thin films, new methodology of transmission electron microscopy, and electronic devices based on oxides and semiconductors.

**John Bell** received his Ph.D. from University of New South Wales and B.Sc. from University of Sydney. Prof. Bell is currently head of School of Chemistry, Physics and Mechanical Engineering at Queensland University of Technology (QUT). Prior to QUT, he was lecturing at the University Technology Sydney. His research operates in interdisciplinary groups and centers, investigating the connections between the underlying structure and the processing, properties, and performance of materials. Other research interest is to develop solutions to make buildings more energy efficient by improving thermal performance, daylight and adopting integrated PV systems which rely on solar energy.